CHAPTER SIX

EXPERIMENTAL RESULTS

6.1 INTRODUCTION

This chapter examines collectively the experimental results. The main focus is on the Laves phase formation and its dissolution and how it affects the mechanical properties of the AISI type 441 ferritic stainless steel. To gain a better understanding of the embrittlement effect from the Laves phase, the results are divided into three parts:

1. microstructural analysis from the failure of materials to understand the source of this embrittlement;
2. effect of the annealing treatment on the Laves phase precipitation and, therefore, its embrittling effect; and
3. the kinetics of the Laves phase formation, and the parameters (such as, temperature and composition) that affect its formation.

6.2 MICROSTRUCTURAL ANALYSIS OF AN AISI TYPE 441 FERRITIC STAINLESS STEEL

In order to understand the source of embrittlement in this steel, microstructural analyses were carried out. These analyses range from simple optical microscopy to more complex transmission electron microscopy analysis. The analyses were carried out on the ferritic stainless steel AISI type 441, and particularly on Steel A that had failed during processing. As it has previously been determined by Columbus Stainless, the source of embrittlement was apparently not grain size related, as the grain size was measured to be 24.8 ± 4.2 μm which is still considered to be fine enough not to have embrittled this material, see Figure 6.1(a). The general grain microstructure had a pan cake structure with the grains elongated in the rolling direction. The scanning electron microscopy (SEM) micrographs show the presence of the grain boundary and matrix precipitates, see Figure 6.1(b).

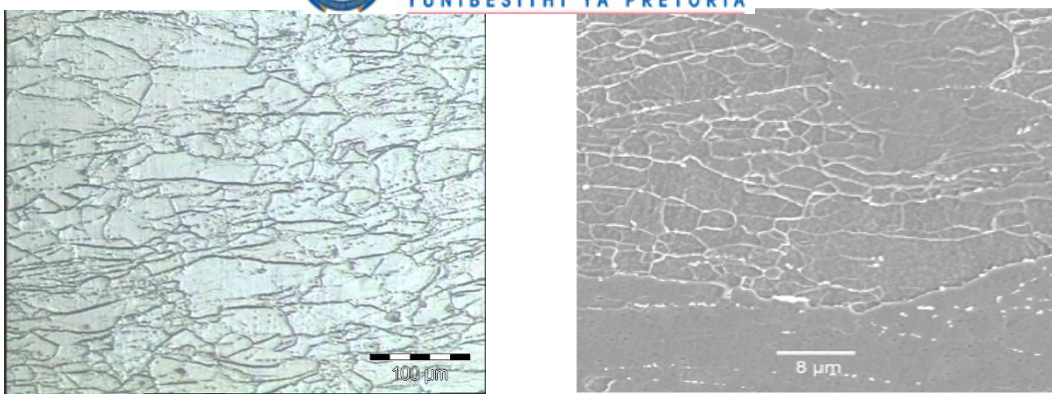

(a) (b)

Figure 6.1. Micrographs from Steel A in the as received hot rolled condition, showing the grain structure. (a) optical microscopy image and (b) SEM images. Note the large difference in magnification with figure (a) showing the "particle decorated" grain structure while figure (b) shows primarily the "particle decorated" subgrain structure.

6.2.1 PRECIPITATE'S IDENTIFICATION

The morphology of the various precipitates in this Steel A changes with the choice of annealing treatment, as revealed by the two types of precipitates (that is, by relative size) that was observed from the SEM micrographs in Figure 6.2. Only the large particles could be analysed successfully using the SEM energy dispersive X-ray technique while the small precipitates were too fine for even a representative semi-quantitative analysis. The large precipitates were found to be most likely a titanium carbo–nitride, which had varying degrees of smaller niobium carbo–nitride precipitates clustered around it and the central precipitate's size was in the region of 2 to 10 μm, see Figure 6.3. According to Gordon and van Bennekom [55], they have reported that the colour of the carbo – nitride changes with the ratio of N/C in the steel. A yellow/orange colour indicates a Ti(C,N) as found in this steel that contains about 10 at. % TiC, see Figure 6.2(a).

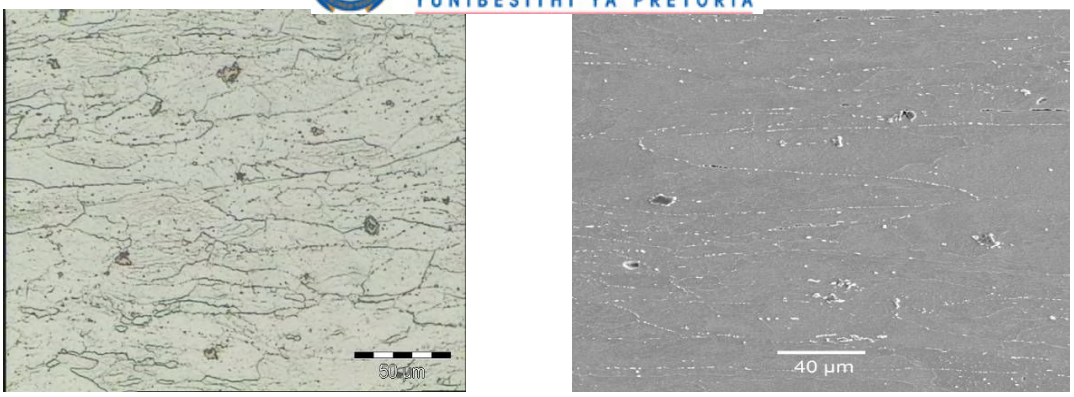

(a) (b)

Figure 6.2. Micrographs of the as received hot rolled Steel A showing its grain structure. (a) An optical microscopy image and (b) a SEM image.

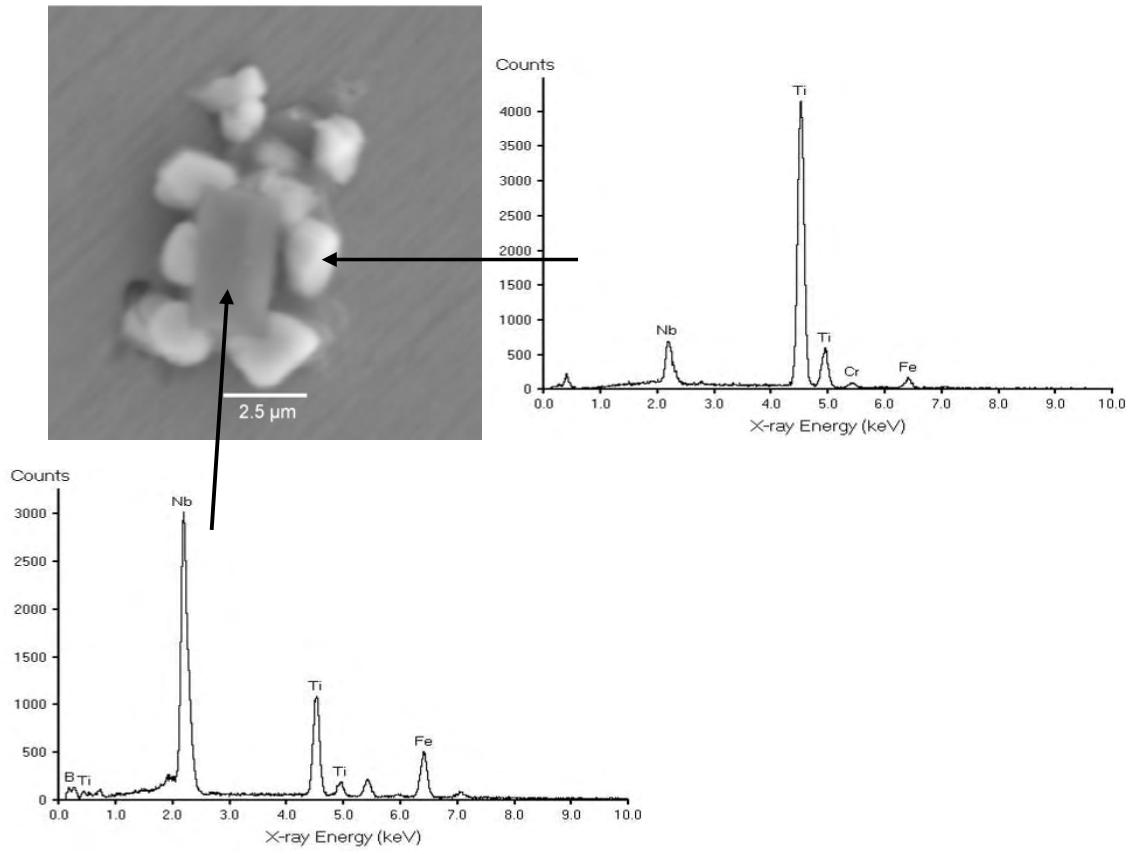

Figure 6.3. SEM – EDS micrograph showing a precipitate consisting of a central cubic core of a mainly titanium containing particle surrounded by a cluster of niobium precipitates.

The SEM results confirm the predictions made by Thermo-Calc®, in that both nitrides and carbides are formed as complex FCC (Ti,Nb)(C,N) precipitates with the Ti(C,N) nucleating first and then the Nb(C,N) nucleating on its surface as a shell or alternatively as a cluster of loose particles around the Ti(C,N). This is not surprising as Ti(C,N) is

known to have a lower solubility in these steels than Nb(CN) and will, therefore, form first during cooling from the melt while the Nb(CN) subsequently forms at slightly lower temperatures by heterogeneous nucleation on the existing Ti(CN). Furthermore, in the work done by Craven et al.[130], they also observed that the (Ti,Nb)(C,N) complex has a least soluble core consisting of TiN that precipitates at higher temperatures during cooling from the melt, and the Nb/Ti ratio in the core is markedly affected by the cooling rates during solidification and later thermomechanical processing.

The small precipitates, however, were analysed using transmission electron microscopy (TEM) and XRD techniques. To be able to analyse the types of precipitates present in this steel without any interference from the matrix, carbon extraction replicas of the precipitates were used and TEM energy dispersive X-ray spectrometer (TEM-EDS) and electron diffraction patterns were used in identifying these precipitates. The transmission electron microscopy (TEM) micrographs for the as received hot rolled Steel A are shown in Figure 6.3. Three types of precipitates were analysed from this specimen;

1. large plate–like precipitates (analysis 1);

2. needle – like precipitates (analysis 2); and

3. small plate-like precipitates (analysis 3),

while there were some fine globular precipitates that could not be accurately analysed using both of these techniques because of their small size. In the work done by Fujita et al [6] it was suggested that the intensity ratio of niobium to iron, Nb/Fe in EDS analysis for the M_6C (Fe_3Nb_3C) type carbide is larger than that for Laves phase (Fe_2Nb). This suggests that large plate – like precipitates (analysis 1) are the M_6C carbide and both the needle–like and small plate–like particles (analyses 2 and 3) are the Laves phase Fe_2Nb. Both M_6C type carbide and Laves phase particles include small amounts of titanium and chromium. However, the amounts of titanium and chromium in both precipitates are much less than those of niobium and iron. From these observations it can be concluded that the composition of the M_6C and Laves phase precipitates are most likely to be $(Fe,Cr)_3(Nb,Ti)_3C$ and $(Fe,Cr)_2(Nb,Ti)$, respectively.

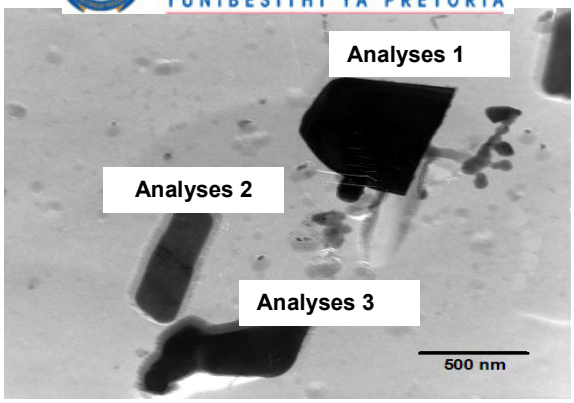

(a)

Analyses 1 | Analyses 2 | Analyses 3

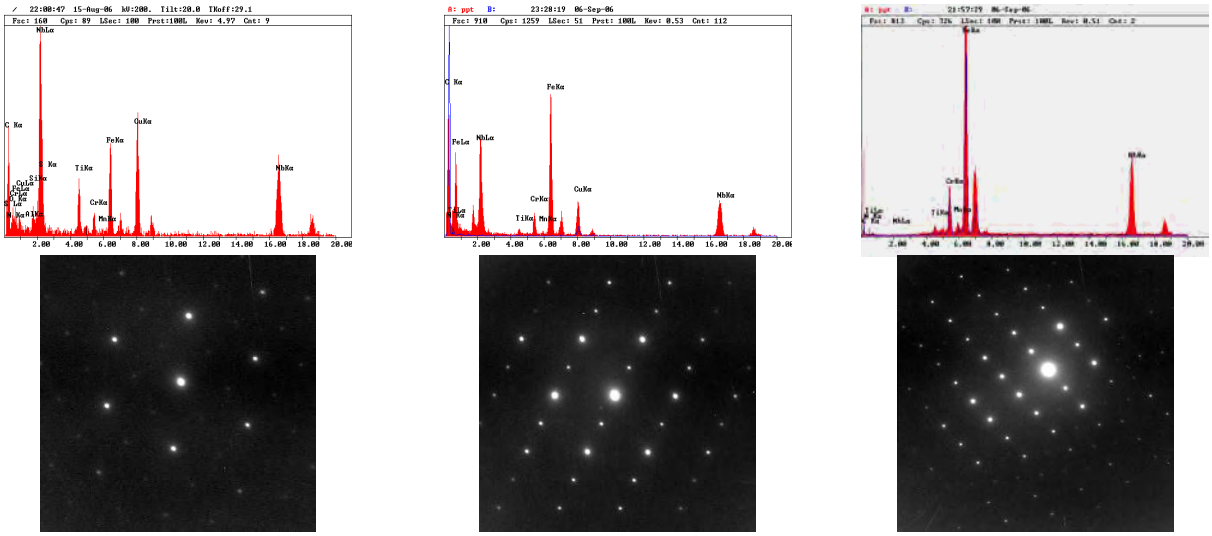

Fe_3Nb_3C [$\bar{1}11$] | Fe_2Nb [$\bar{1}00$] | Fe_2Nb [$10\bar{2}$]

(b)

Figure 6.4. Transmission electron micrographs of particles from extraction replicas and their analyses by electron diffraction and EDS of the as-received hot rolled Steel A showing different particle morphologies.

The diffraction patterns of the large globular precipitates (analysis 1) show a cubic crystal structure with a lattice parameter a_o = 1.11 nm. Therefore, these precipitates are identified as most likely to be cubic M_6C carbides. On the other hand, the diffraction patterns of the needle-like or elongated phase (analysis 2) and plate-like precipitates (analysis 3) show the crystal structure to be most likely identified as hexagonal. The lattice parameters were measured to be a_o = 0.48 nm and c_o = 0.79 nm, with c_o / a_o = 1.64, which is close to the $MgZn_2$ C14-type of the Laves phase.

Figure 6.5 shows the results of the XRD analyses of the precipitate residues after electrolytic extraction from the as received material, Steel A. Two main types of precipitates where detected, i.e., the Laves phase and the carbo-nitrides, but there was a small amount of M_6C carbides also present, as was also found in the TEM analysis. From Figure 6.5 , the peaks for the M_6C phase is not clearly visible, but when the Rietveld refinement approach was used to quantify these phases, its presence was detected as a small amount. Note, however, that it is not always possible to get a fully pure precipitate extraction of precipitates without the interference of the matrix material, the α-Fe matrix phase is considered to be also present in this measurement. Table 6.1 shows the weight fractions of the precipitates present in this steel, with the error calculated as a 3 sigma error (meaning three times the standard deviation). The volume was calculated using the densities of each phase and the total mass of precipitates' residue extracted from the steel by weighing. The results indicate that the normalised weight fractions for the Laves phase and (Ti,Nb)(C,N) to be about 1.14% and 0.33%, respectively.

Using the Rietveld refinement approach, the lattice parameters of the Laves phase were determined to be a_o= 0.481 nm and c_o = 0.784 nm and these values are close to the ones determined above from the TEM diffraction patterns.

Table 6.1. The measured weight fractions of the precipitate phases found in the as received hot – rolled material, Steel A.

	XRD analysis		Calculated values			
Phase	Weight fraction (%)	3 σ	Weight phase (g)	Normalised weight frac. (%)	Density (g/cm^3)	Vol. (x $10^{-3}cm^3$)
Fe_2Nb	56.36	2.04	0.037	1.143	8.63	1.32
M_6C	2.02	0.66	0.001	0.041	8.44	0.05
α - Fe	16.24	0.84	0.011	0.329	7.87	0.42
(Ti,Nb (C,N)	25.39	2.52	0.017	0.515	7.82	0.80

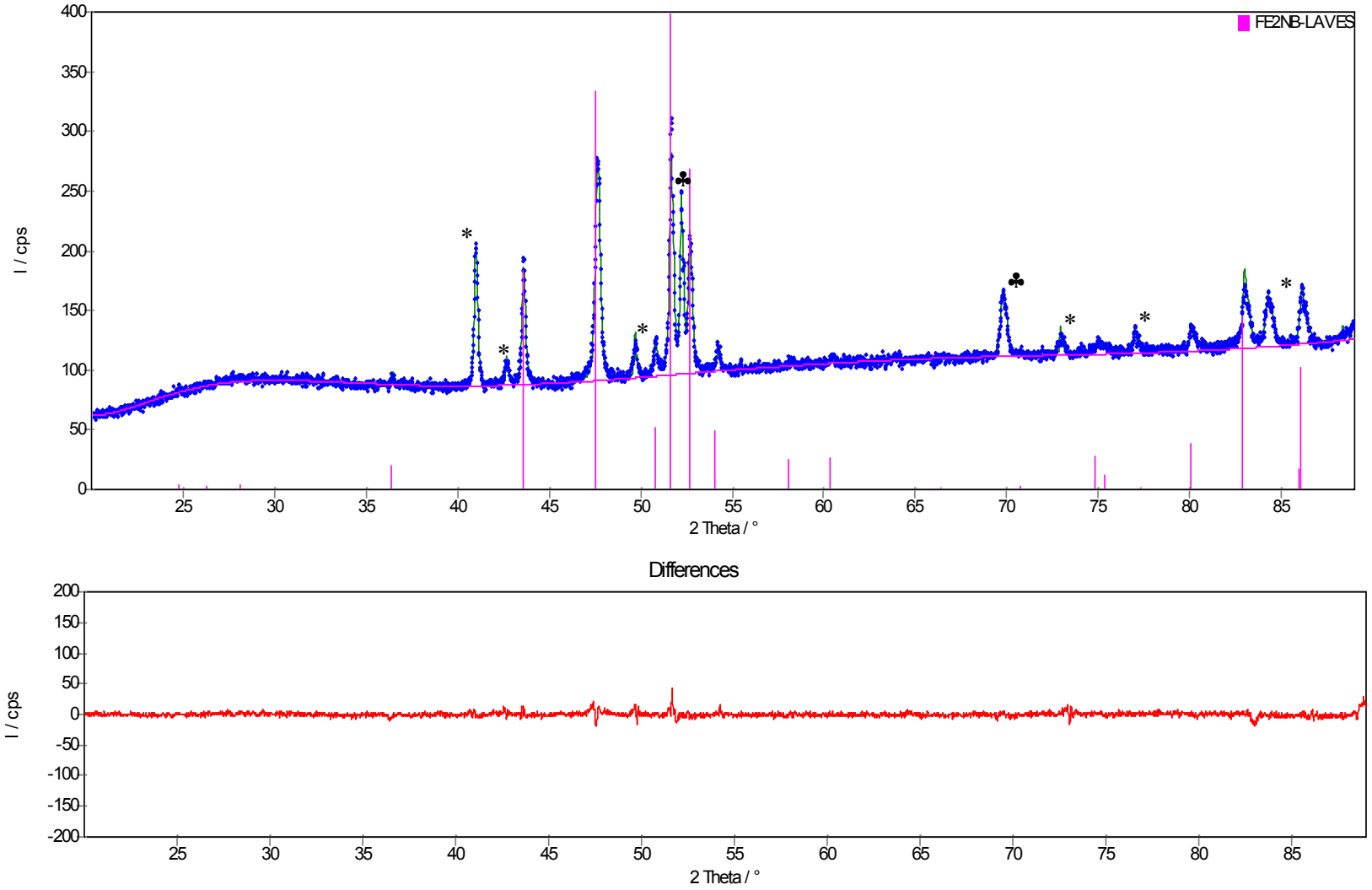

Figure 6.5. A typical XRD scan of the precipitate residue after electrolytic extraction from Steel A, i.e. the as received material, showing the presence of the Laves phase peaks (indicated by the lines in the top figure). The remaining peaks are the carbides and nitrides, indicated by (∗) and the α - Fe matrix, indicated by (♣). Note the good residual difference between the calculated and the measured spectrum as is shown by the spectrum below.

Fujita et al., [101] using the *MTDATA* thermodynamic software, have modelled the precipitation kinetics in the Fe-Nb-C system for a 9Cr-0.8Nb steel at 950 °C. They have observed that the atomic ratio of Fe to Nb in the extracted residue in their steel approaches unity with increasing ageing time, and this indicates that the Laves phase (Fe_2Nb), which contains more iron than required by stoichiometry in Fe_3Nb_3C, dissolves to give way to Fe_3Nb_3C. This meant that the Laves phase was a metastable phase that gave way to the precipitation of Fe_3Nb_3C, and they have suggested that the precipitation sequence towards the equilibrium phases in their high niobium content stabilised ferritic stainless steel to be NbN and Fe_3Nb_3C:

$$\alpha \rightarrow \alpha + Nb(C,N) + Fe_2Nb + Fe_3Nb_3C \rightarrow \alpha + NbN + Fe_3Nb_3C$$

where α represents ferrite. In this study on the embrittled Steel A with a lower niobium content reported here, the Thermo-Calc® prediction did not show this reaction sequence of Fujita et al., [101] because this sequence is a time dependent reaction, and Thermo-Calc® calculations only apply to the phases at full equilibrium. Secondly, the relatively large difference in niobium content between the two steels should also be noted. In order to prevent a great loss in strength during service, it is necessary to control the precipitation sequence during high temperature aging. This can be achieved by reducing the carbon content or by adding some other alloying elements that have a stronger affinity for carbon, and this will impede precipitation of the coarse M_6C carbides.

6.3 Effect of Annealing Treatment on the Microstructural and Mechanical Properties

6.3.1 Microstructural Analysis

Figure 6.6 shows the effect of annealing heat treatment on the grain structure evolution from the as-received hot-rolled material, Steel A. During this process the grain size was measured by the linear intercept method. The microstructural analysis of the as received material shows that full dynamic or static recrystallisation had indeed not occurred during and after hot rolling and, therefore, there was no measurable grain refinement from dynamic recrystallisation during hot rolling. In fact, full recrystallisation was observed to have occurred only at temperatures above 1000 °C. With annealing at

temperatures below 1000 °C, the grain size evolution shows that only recovery had taken place and only a minimal level of grain growth was observed.

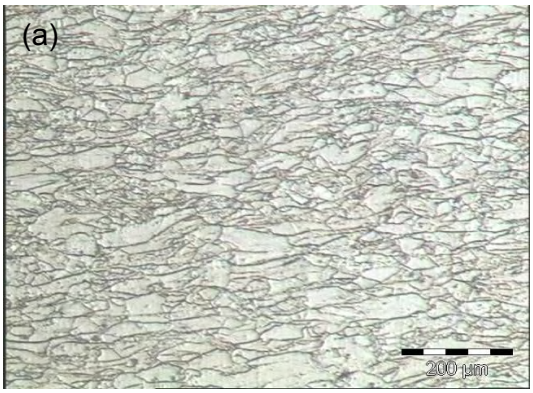

As received

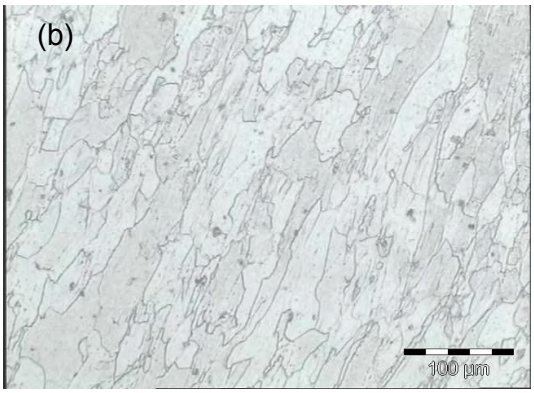

850 °C

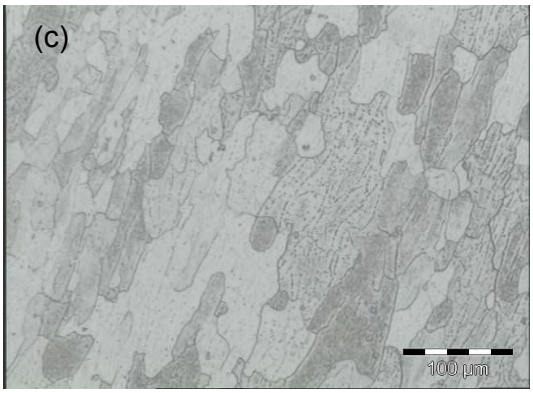

875 °C

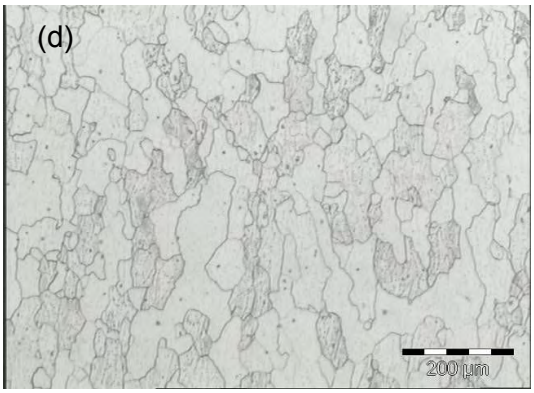

900 °C

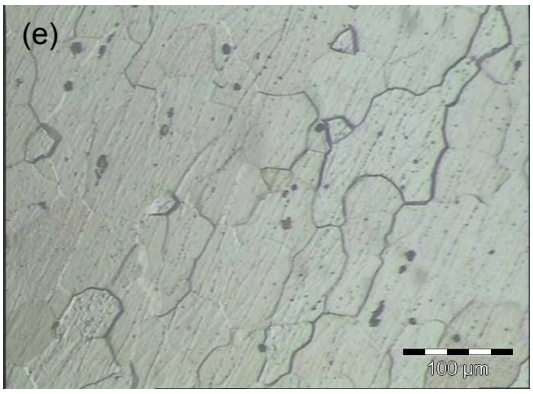

950 °C

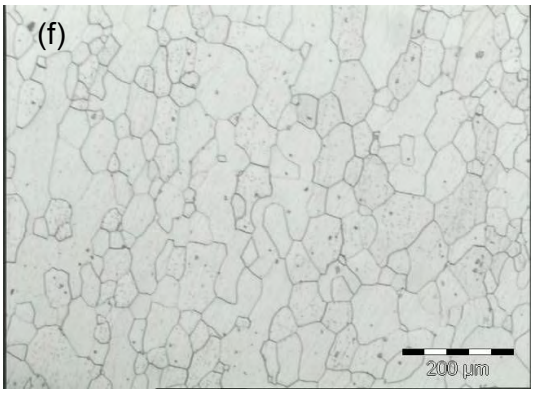

1000 °C

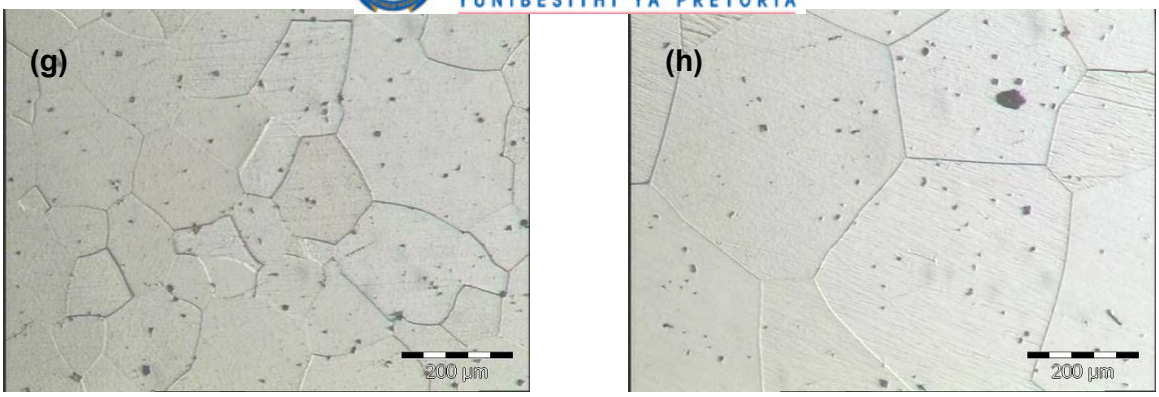

1050 °C **1100 °C**

Figure 6.6. Optical micrographs of the specimens from Steel A after annealing at different temperatures for 30 minutes followed by water quenching (In comparing the microstructures, note the differences in magnifications).

The SEM and TEM results also indicate that the volume fraction of fine Laves phase precipitates tends to decrease as the annealing temperature increases towards the solvus (see Figure 6.7 and 6.9, respectively), as would be expected also from the Thermo-Calc® predictions. Both micrographs show that the Laves phase has precipitated on the sub-grain and grain boundaries and only small amounts are found within the grains. This indicates that the Laves phase possibly nucleates firstly at the sub-grain and grain boundaries and then, only after site saturation, within the grain matrix. With annealing temperatures above 900 °C, complete dissolution of the Laves phase is observed, and the grain's microstructure has fully recrystallised. At annealing temperatures between 700 °C and 850 °C, the TEM micrographs show that there is a higher volume fraction of the grain boundary Laves phase, and these precipitates have coalesced to form stringers. It is these grain boundary precipitates that would later result in embrittlement of this material. In the study done by Sawatani et al [8] the same observation was also made, and they have found that the quantity of the precipitates in their as-hot rolled material, reaches a maximum after being annealed and slowly cooled from about 700 °C but that the volume fraction then decreases with slow cooling from above 900 °C. They have also observed that the Laves phase dissolves into a solid solution at an annealing temperature of over 900 °C, and this finding coincides with the results of the XRD and TEM analyses, where Laves phase was detected only at temperatures up to 850 °C.

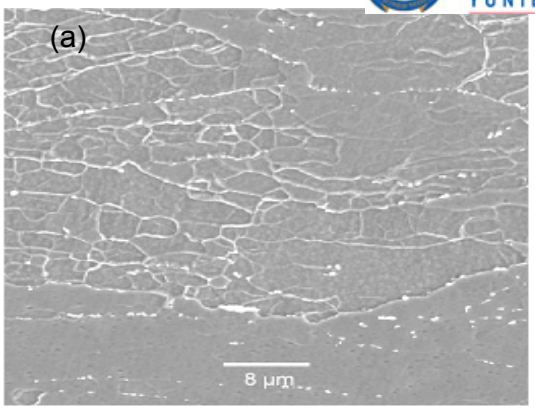

As received

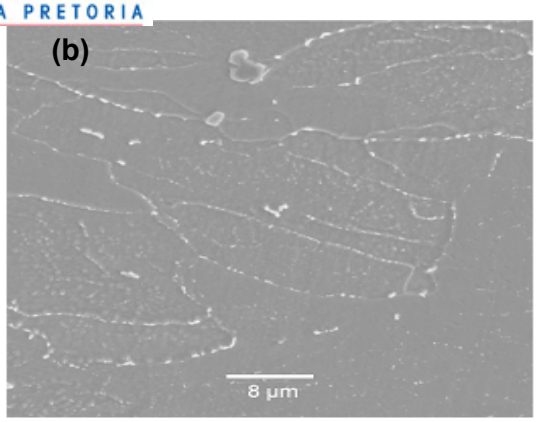

850 °C

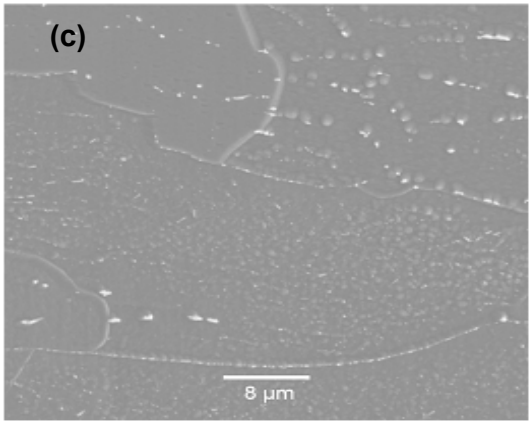

875 °C

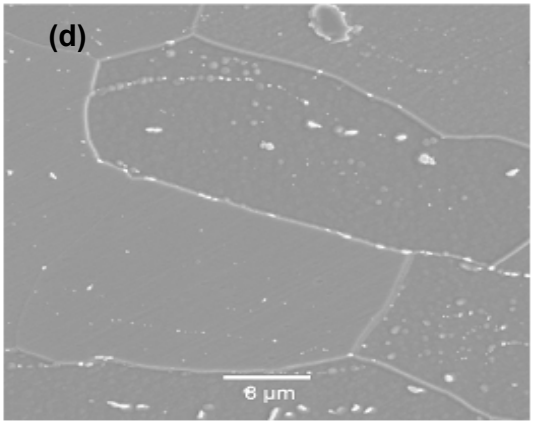

900 °C

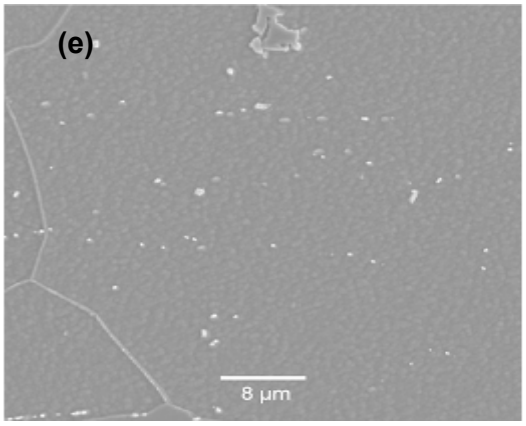

950 °C

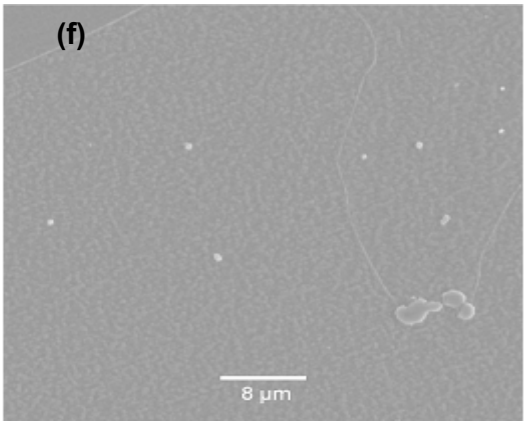

1000 °C

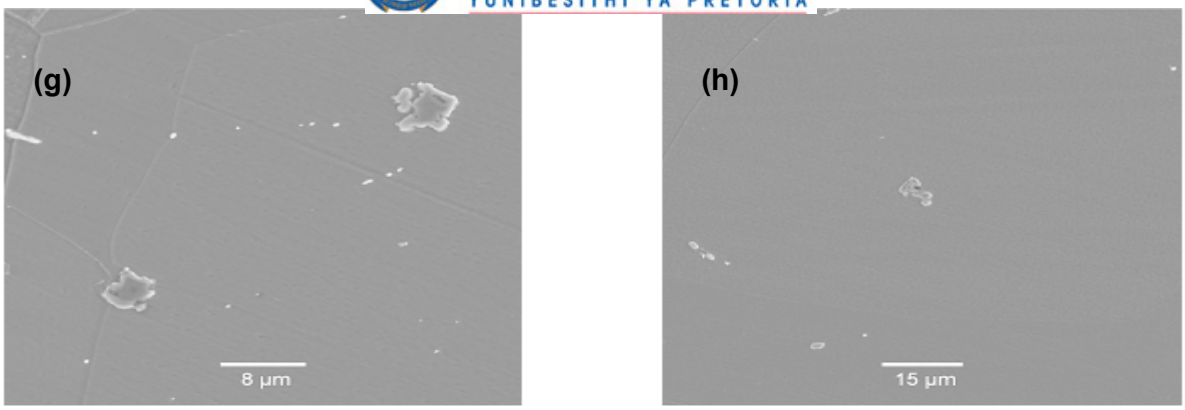

1050 °C 1100 °C

Figure 6.7. SEM micrographs of Steel A showing the effect of annealing temperature on the morphology of the second phase.

As received

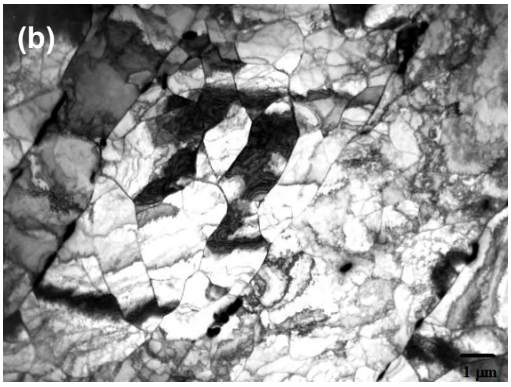

600 °C

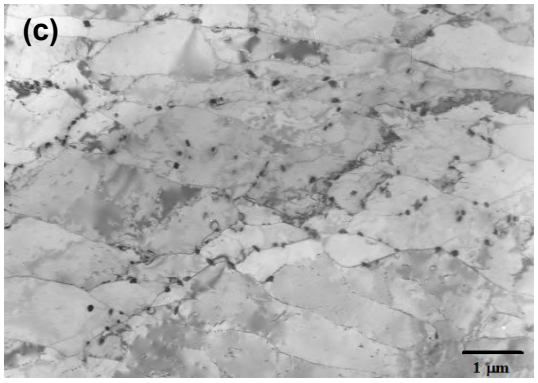

650 °C

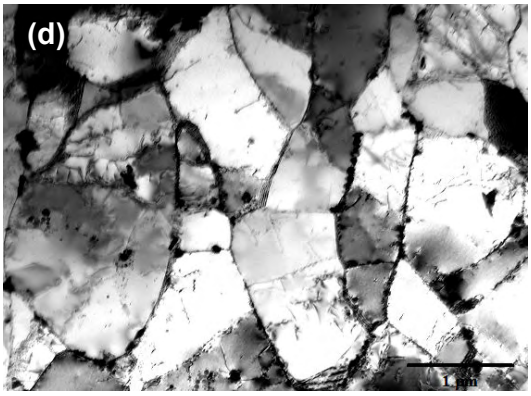

700 °C

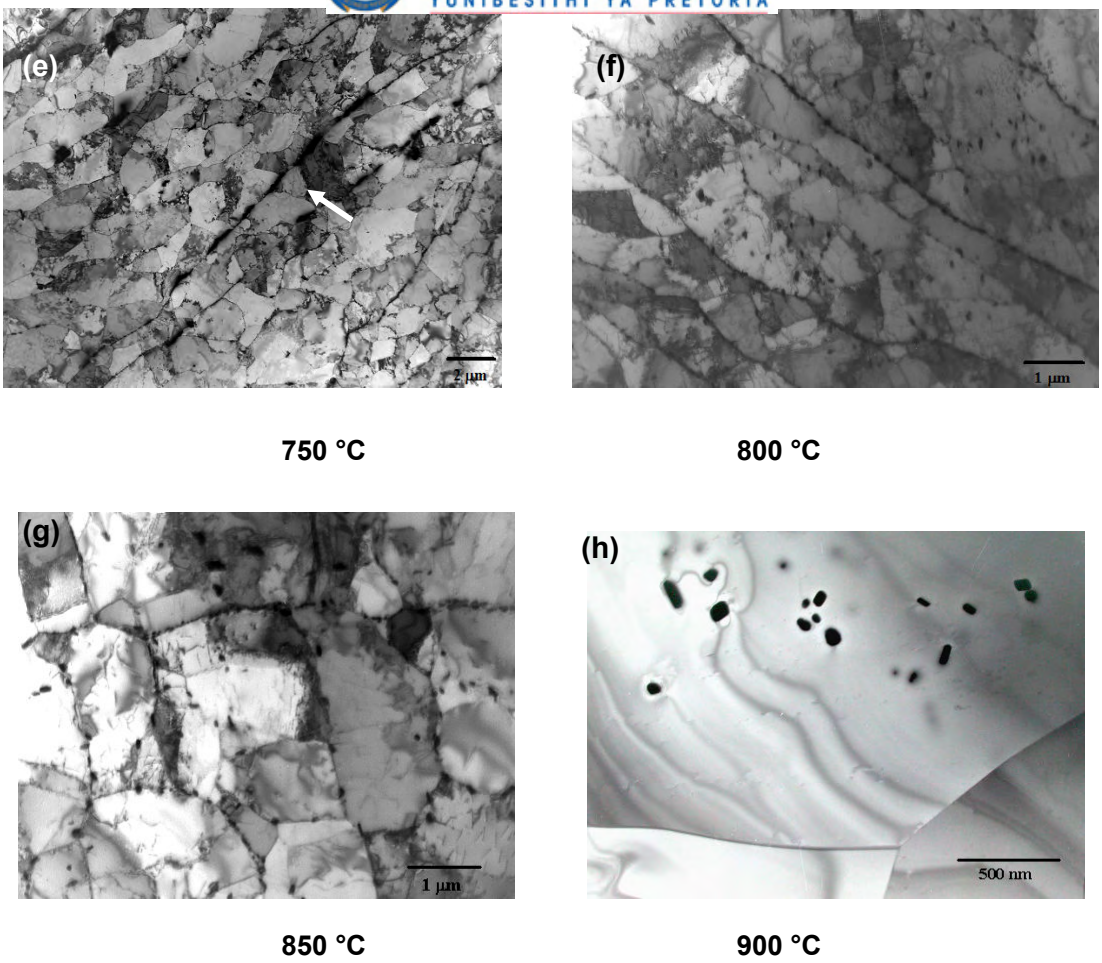

Figure 6.8. TEM micrographs from Steel A showing the presence of the fine Laves phase precipitates on the subgrain boundaries of the specimens that were annealed at the shown different temperatures for 1 hour and then water quenched.

6.3.2 PRECIPITATE'S MORPHOLOGY

Transmission electron microscopy micrographs (TEM) of the dislocation structures in the specimen annealed at 700 °C and then water quenched, are shown in Figure 6.9. The precipitation of Fe_2Nb particles on the dislocations and subgrain boundaries are shown in Figure 6.9 (a & b). The halo surrounding these particles within the grains is believed to be associated with the strain fields surrounding these particles [92]. Nucleation of the Fe_2Nb occurs firstly on grain boundaries, then at dislocations, and at a later stage within the matrix. In the work by Li [131] on the precipitation of Fe_2W Laves phase in a 12Cr-2W alloy, the author observed that Laves phase particles on grain boundaries are coherent with one grain but grow into the adjacent grain with which they do not have a rational orientation relationship. This is due to the higher mobility of the incoherent interface if compared to the semi- or coherent one. This may also be clearly seen in this

Steel A on the "horizontal" grain boundary in the middle of Figure 6.9 (a) where all the Laves phase particles appear to be growing only into the top grain.

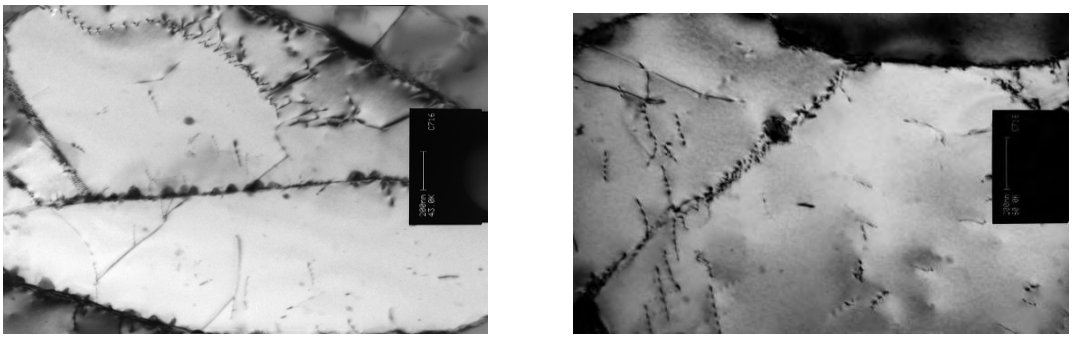

(a) (b)

Figure 6.9. Thin foil electron transmission micrographs from steel A, annealed at 700 ºC for 1 hour and then water quenched. The micrographs show (a) the nucleation of the Laves phase precipitates on grain boundaries and dislocations and (b) some fine matrix precipitates surrounded by a strain halo as well as dislocation nucleated precipitates.

6.3.3 MECHANICAL PROPERTIES

The results from the V-notch room temperature Charpy impact tests on specimens solution treated at different temperatures and water quenched of the process embrittled Steel A, are shown in Figure 6.10. The Charpy Impact Energy (CIE) shows a maximum of about 60 J for the specimens that had been annealed at 850 °C, which coincides with the predicted Laves phase solvus temperature, but with a decreasing CIE with annealing on both sides of this temperature. In the specimens that had been annealed at 900 °C and above where no Laves phase is present, the impact energy averaged only about 10 J. It can be concluded that above 850 °C, a grain size effect from grain growth plays a major role in lowering the impact energy, but below 850 °C, the precipitation of the intermetallic Laves phase contributes to the lowering of the impact toughness. Comparing these results with the prediction from Thermo-Calc® (Section 5.7), it can be seen that as the volume fraction of the Laves phase decreases in the steel with a rise in the annealing temperature towards 850 °C, the impact toughness also increases to its maximum of 60 J at 850 °C. Beyond 850 °C grain growth plays a major role in embrittling this ferritic steel, a problem that is well known in most ferritic stainless steels.

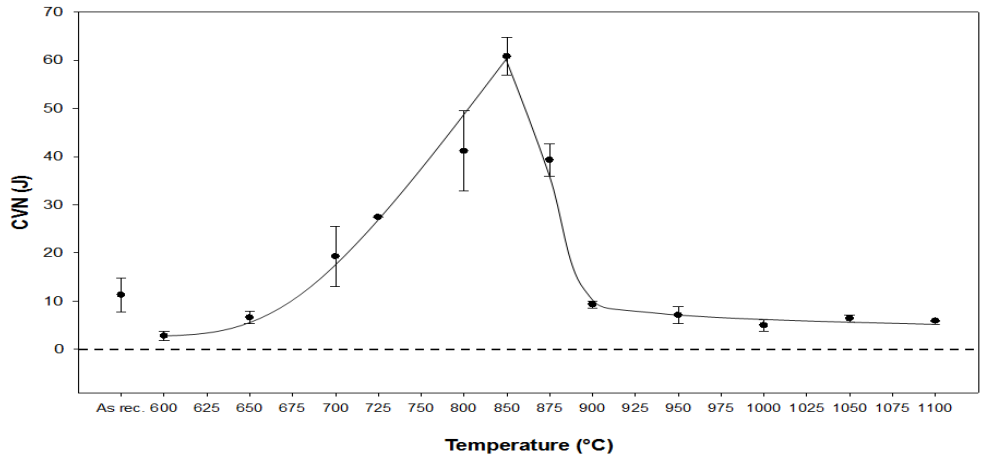

Figure 6.10. Effect of annealing temperature on the room temperature Charpy impact energy of the as hot rolled and annealed AISI 441 stainless Steel A. The samples were annealed for 30 minutes and then water quenched.

Typical fracture surfaces from specimens after annealing at different temperatures are shown in Figure 6.11. In Figure 6.11 (a) the micrograph is shown of the as received and process embrittled Steel A with a CIE of only slightly above 10 J, with the fracture surface showing both macro- and micro-voids in a dimpled surface, which is characteristic of a ductile failure although the CIE was actually relatively low. The (Ti,Nb)(C,N) particles are readily identifiable as “blocky” precipitates, as clearly seen in Figure Figure 6.12 (b). These macro-voids appear to be formed by the presence of these large cuboidal particles which indicates a low cohesive force between these carbo-nitride precipitates and the steel matrix. These precipitates are, therefore, possibly not the direct cause of the brittleness of the alloy. The presence of the Laves phase on the grain boundaries (see Figure 6.7 and Figure 6.8 (as received)) must then have contributed to the brittleness of these materials, but the exact mechanism could not be revealed from the fractured surface analysis.

Figure 6.11 (c & d) show the fractographs of the specimen that had been annealed at 850 °C where the maximum CIE was found, indicating that fracture had occurred in a ductile manner. Noticeable, however, are the large numbers of voids situated on a few of the grain boundaries in Figure 6.11 (d), indicating the presence of particles on some of these grain boundaries, most likely the last remaining Laves phase. There are, however, no further significant or obvious differences in the observed failure mode between the hot rolled as received material with a CIE of only about 10 J and the sample annealed at 850 °C with a CIE of 60 J, except that there are also a few Laves phase precipitates present on the grain boundaries of the as received steel (see Figure 6.7(a))

whereas the steel annealed at 850 °C, according to Thermo-Calc® should have had no Laves phase in its microstructure. Previous studies have shown that the presence of the Laves phase degrades the mechanical properties of this high chromium ferritic steel where ever this phase is formed within the temperature range of 500 – 750 °C [132]. Figure 6.11 (e & f) show the fracture surfaces of the specimen that had been annealed at 900 °C; which shows transgranular cleavage fracture with individual grains identified by changes in the directions of the river markings. Figure 6.11(f) shows the specimen displaying microcracks that are clearly visible on the fracture surface. Evidence suggesting cleavage or grain boundary microcracking was occasionally observed, but little role of microstructure in the crack initiation process could be directly observed.

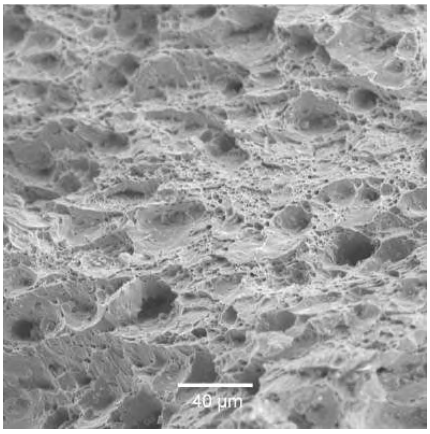

(a)

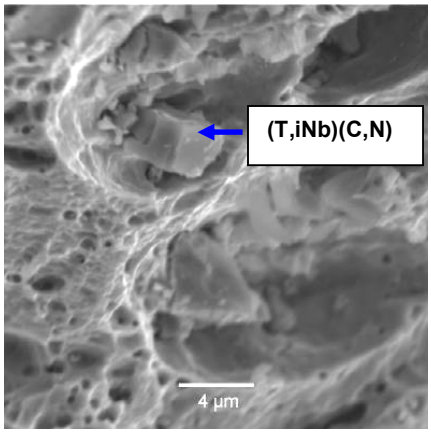

(b)

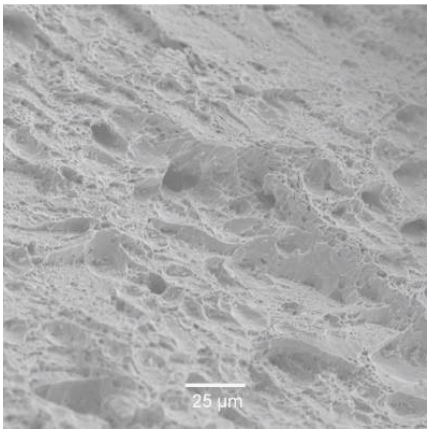

(c)

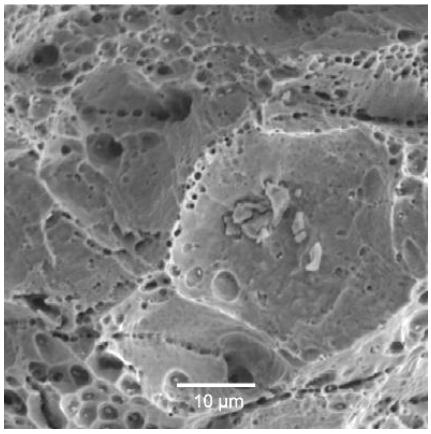

(d)

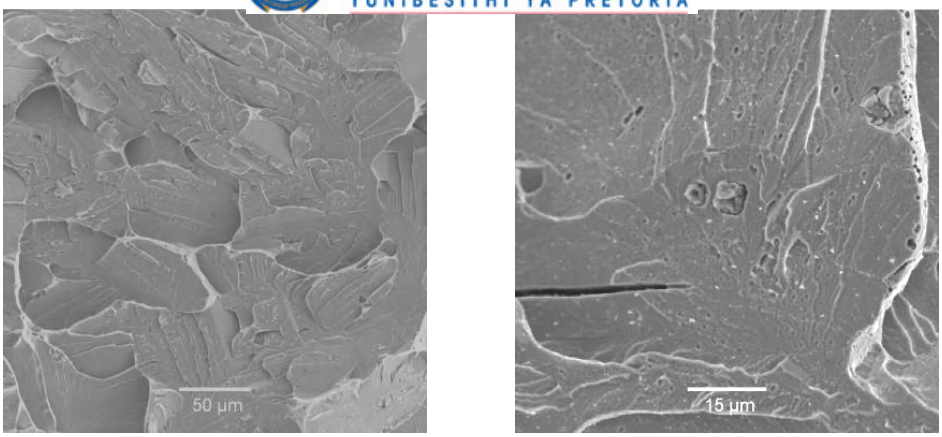

(e) (f)

Figure 6.11. Examples of the Charpy fracture surfaces at different magnifications of steel A (a & b) from the as received specimen; (c & d) after annealing at 850 °C; and (e & f) after annealing at 900°C.

6.3.4 Effect of Grain Size on the Mechanical Properties of Steel A

Figure 6.12 shows the variation of the hardness and grain size as a function of the solution annealing temperature above 850 °C, i.e. where there should not be any Laves phase present in the Steel A but where grain growth is expected. The results indicate that there is a steady decrease in the Vickers hardness whereas the as-received and brittle hot-rolled steel shows a much higher hardness than that of the specimens that had been annealed in the grain growth region. This can not be attributed purely to the grain growth effect since there is only a relatively small difference in grain size between the as-received hot rolled material and the specimen that had been laboratory annealed at 850 °C after hot rolling. This difference in hardness may, however, arise from accumulated strains induced during the hot rolling process in the as received steel, particularly if full dynamic recrystallisation had not occurred. The microstructural analysis of the as received material shows that full dynamic recrystallisation had indeed not occurred, and therefore, there was no measurable grain refinement from dynamic recrystallisation, see Figure 6.13. The presence of the fine grain size and the Laves phase could have contributed to a much higher hardness value of the as received material; but as the steel is further annealed, recrystallisation starts to occur and thereby softens the steel.

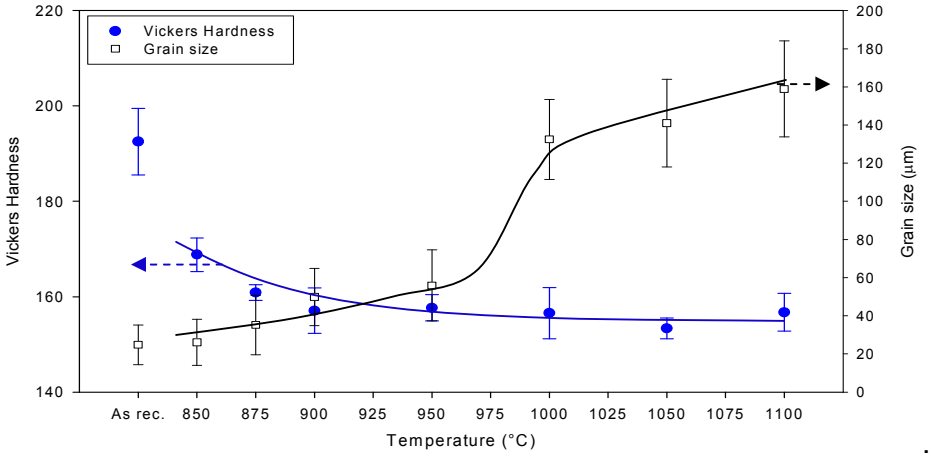

Figure 6.12. Effect of annealing temperature above 850 °C on the grain size and Vickers hardness for the AISI type 441 ferritic stainless Steel A.

Figure 6.13. TEM micrograph showing the presence of a dislocation substructure and some fine Laves precipitates in the as received hot rolled specimen of Steel A, indicating a lack of full dynamic recrystallisation during the last stage of hot rolling.

The results also show that there is a steady increase in grain size up to about 950 °C, but between 950 °C and 1000 °C there is a sudden and rapid 60 % increase in the grain size. The TEM micrographs of the specimens that were annealed at 850 °C and 900 °C respectively, with the presence of some remnants of Laves phase in the specimen that was annealed at 850 °C, were shown in Figure 6.8. At 900 °C this phase had completely dissolved, see Figure 6.8 for the microstructural evolution during annealing at these temperatures.

Figure 6.14 shows the effect of annealing temperature at and above 850 °C on the tensile properties of the Steel A. Both the 0.2 % offset yield strength and ultimate tensile strength (UTS) decrease whilst the percentage elongation increases with increasing annealing temperature. Significantly, however, the specimen that had been heat treated

at 850 °C shows a relatively poor elongation whereas at 900 °C the elongation had already increased significantly, confirming that at 850 °C some last remaining and embrittling Laves phase was still present while at 900 °C it had completely dissolved. The effect of grain growth on the 0.2% yield strength in this steel was tested according to the Hall-Petch relationship, and was found that it only applies in the temperature range of 850 °C to 950 °C but beyond 950 °C, the relationship did not hold.

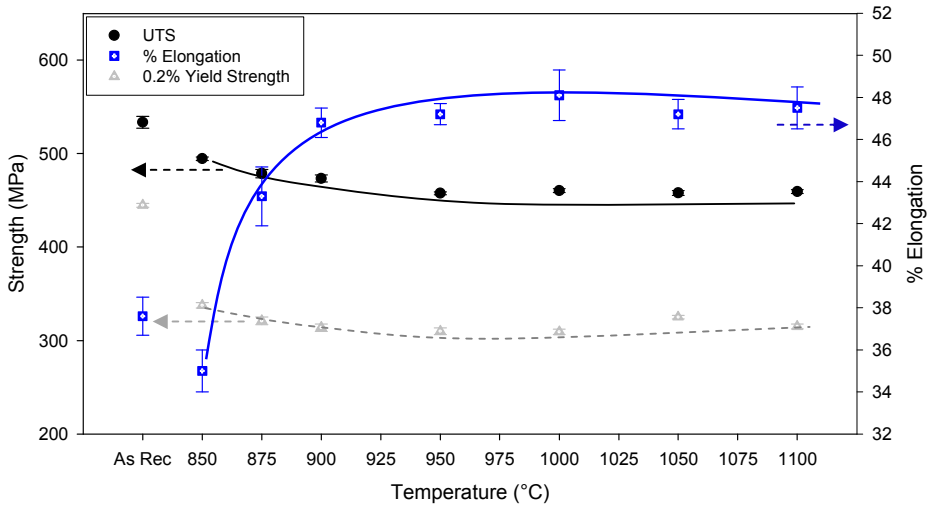

Figure 6.14. Effect of annealing temperature at 850 °C and above on the tensile strength and elongation of the 441 stainless steel A.

6.4 Effect of Annealing Treatment on the Charpy Impact Energy and DBTT

The results of Charpy impact tests at various testing temperatures on the heat treated specimens of this 441 ferritic stainless steel (Steel A) are shown in Figure 6.15. The specimens were initially annealed in the temperature range of 600 to 950 °C for 30 minutes and subsequently quenched in water. The specimen that was quenched from 850 °C exhibits a maximum toughness of about 60 J at 25 °C and a Ductile Brittle Transition Temperature (DBTT) of about 5 °C at about 30 J. Solution treatment at 950 °C resulted in the DBTT to be as high as 40 °C, in comparison with the steel treated at 850 °C while all these specimens fractured in a brittle manner. On the other hand, the upper shelf energy for the specimen solution treated at 950 °C was found to be much higher, averaging about 90 J.

The grain size of the heat treated samples varied from about 22 to 60 µm as the annealing temperature was increased from 850 to 950 °C (see Figure 6.15). The DBTT was observed to rise with increasing grain size from both specimens, but the upper shelf energy seemed to be independent of the grain size. This could be caused by the

presence of some Laves phase on the grain boundaries still present in the specimen that was annealed at 850 °C, resulting in lowering the upper shelf energy to about 60 J compared to 90 J in the specimen that was annealed at 950 °C.

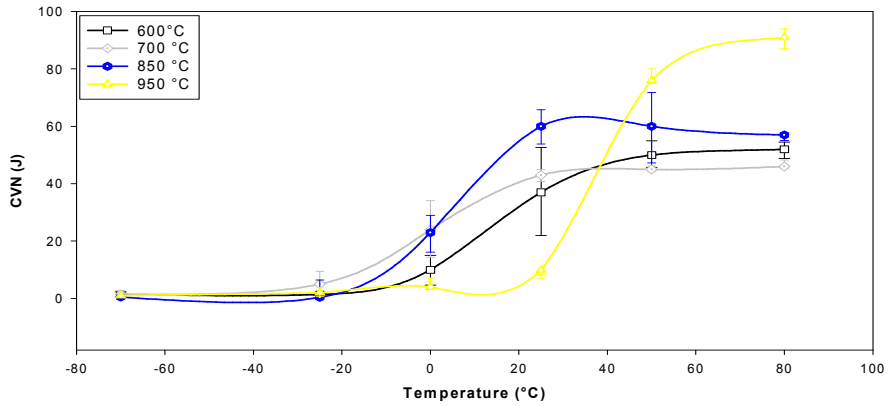

Figure 6.15. Charpy impact energy of the 441 ferritic stainless steel A as a function of the test temperature from specimens that were annealed at four different temperatures, both within and outside the Lave phase formation region.

6.5 Effect of Re –embrittlement treatment on The Room Temperature Charpy Impact Energy

6.5.1 Effect Of Cooling Rate

The effect of cooling rate on the room temperature impact toughness of the steel after annealing at 850 °C and 950 °C respectively for 5 min in the Gleeble simulator followed by forced helium cooling at different linear cooling rates, is shown in Figure 6.16. The aim of this exercise was to simulate the effect of the post-hot rolling cooling rate on the final grain size and on the precipitation of Laves phase and hence their impact on the Charpy impact energy to provide process guidance on the importance of rapid cooling rates after the final stage of hot rolling. As observed before, rapid cooling from 850 °C gives a higher impact energy than after cooling from 950 °C, and this is caused initially by a difference in grain size. This can be observed from the specimens that were subject to cooling rates of about 50 °C/s, where there was a difference of 34 J in the upper shelf energy between the specimens annealed at 850 °C and 950 °C respectively, see Figure 6.16, with results that are comparable to those in Figure 6.10. Note furthermore, that the impact strength after cooling from 950 °C is only marginally affected by differences in cooling rate while this is not so after cooling from 850 °C where faster cooling results in smaller volumes of Laves phase forming during cooling

and, hence, in higher impact strengths. This difference is significant as it proves that the embrittling effects of a large grain size introduced by cooling from 950 °C, overrides any further embrittlement by Laves phase caused by slow cooling. Embrittlement in these ferritic stainless steels from a larger grain size, therefore, appears to be even more deleterious than that of Laves phase if both are present together.

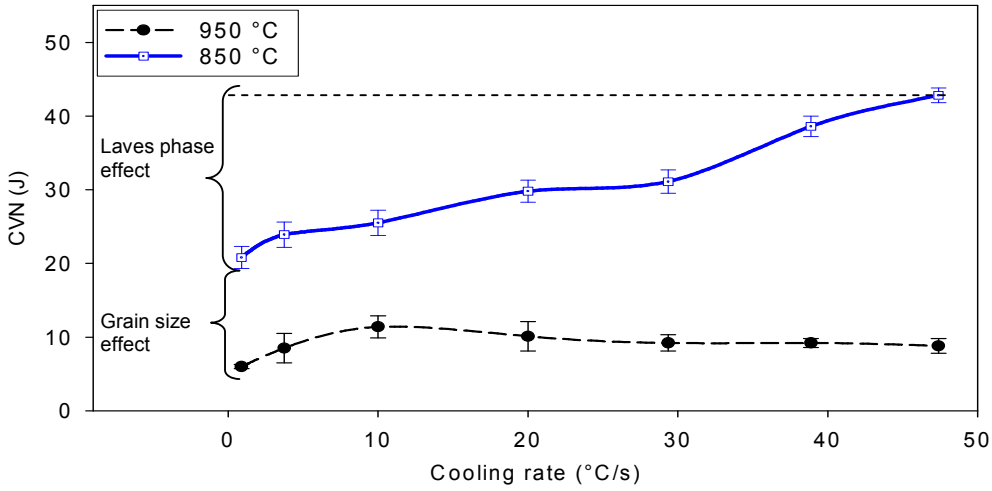

Figure 6.16. Effect of linear cooling rate in °C/s on the room temperature impact toughness of the specimens from Steel A that were cooled at linear cooling rates from 850 °C and 950 °C, respectively.

In relation to the observed toughness behaviour, the Laves phase precipitation behaviour was considered. The metallurgical observation from the two samples that were solution treated at these temperatures and cooled at 60 °C/s, shows two completely different microstructures, see Figure 6.17. After solution treatment at 850 °C, the microstructure has not recrystallised and the electron micrograph shows the presence of a subgrain structure in Figure 6.17 (a & b). Solution treatment at 950 °C, however, shows that the microstructure has now fully recrystallised and is without any subgrain structure in Figure 6.17 (c & d). In both cases, there are few large particles still present that were analysed as niobium carbo-nitride, Nb(C,N) using TEM EDX.

Figure 6.18 shows the effect of the cooling rate on the precipitation of the Fe_2Nb Laves phase after cooling at a rate of 1 °C/s. Figure 6.18 (a & b) show a band of fine precipitates from the samples that were solution treated at 850 °C and 950 °C and then cooled slowly, respectively. Note that these fine precipitates are found on the grain boundaries in the sample that was solution annealed at 850 °C, whereas in the sample that was solution treated at 950 °C, these precipitates where observed within the grains.

This suggests that the Laves phase can precipitate homogeneously in a coarse grain microstructure. The volume fraction of the Laves phase in the steel decreases with increasing cooling rates, as seen in Figure 6.17 and Figure 6.18. From this investigation, the quantitative work on the amount of the Laves phase precipitated from the two solution annealing temperatures was then carried forward.

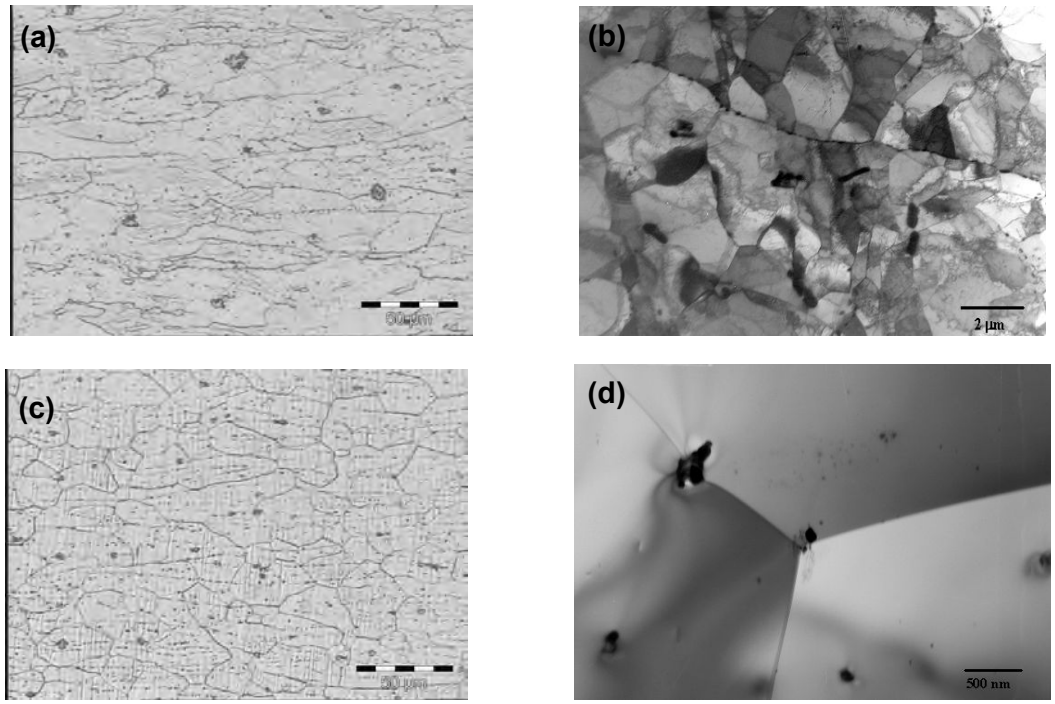

Figure 6.17. TEM micrographs of the samples of Steel A that were solution annealed at 850 °C and 950 °C for 5 min then cooled at 60 °C/sec. (a & b) solution treated at 850 °C; (c & d) solution treated at 950 °C. Note the differences in the microstructures from both samples.

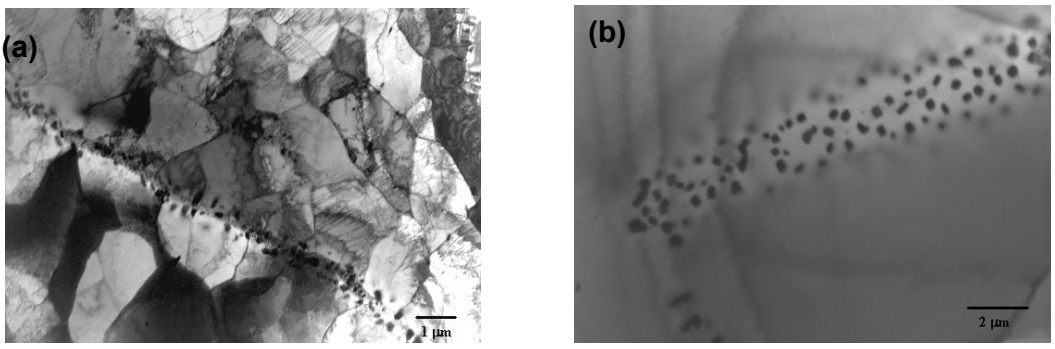

Figure 6.18. TEM micrographs of the samples from Steel A after being cooled at 1 °C/sec from: (a) solution annealed at 850 °C and (b) 950 °C for 5 min before cooling.

The effect of the cooling rate on the amount of Laves phase precipitated from the specimen annealed at 850 °C is shown in Figure 6.19. As the cooling rate increases, the amount of the Laves phase formed decreases and the Charpy impact value

increases (see Figure 6.16). This serves as evidence showing that the volume fraction of the Laves phase plays an important role in embrittling this steel. In the work by Sawatani et al.[8], they have also found that a large amount of fine Laves phase nucleates first at the grain boundaries and then within the grains during cooling. As the cooling rate becomes lower, the amount of Laves phase that forms increases, as would be expected. These large amounts of precipitates were found to increase the strength and decrease the elongation [8,69], whilst also decreasing the toughness of the steel. The toughness and ductility can be recovered by heating the material again to above 900 °C to dissolve the Laves phase, followed by rapid cooling.

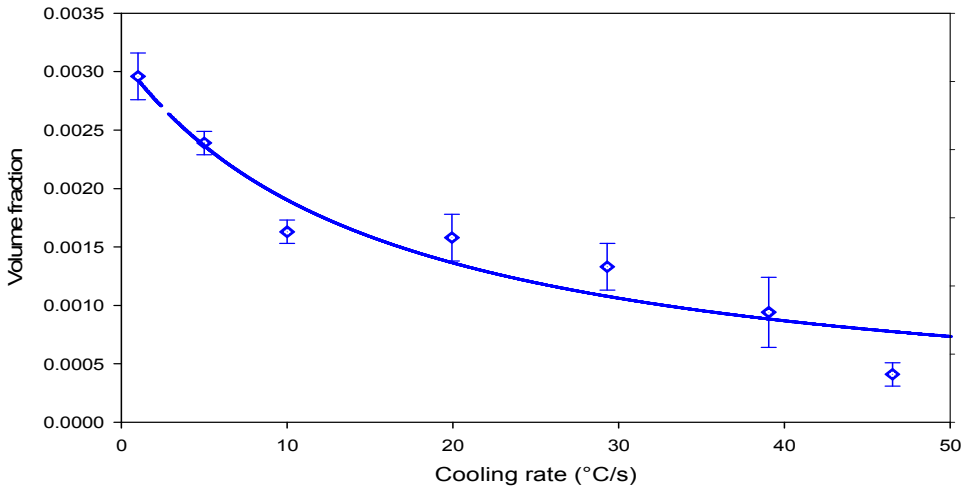

Figure 6.19. Effect of the cooling rate on the volume fraction of the Laves phase in Steel A after cooling at different rates from annealing at 850°C.

6.5.2 Effect of the Reheating Treatment

The results of the Steel A samples that were reheated at 600 °C to 900 °C for 30 minutes after being solution treated at 950 °C for 1 hour, are shown in Figure 6.20. The aim of these tests was to dissolve the Laves phase completely and then re–precipitate them at the different annealing temperatures. After the reheating treatment, all the samples show a significant decrease in both ductile-to-brittle transition and upper-shelf energy. All the samples that were supposed to be embrittled have a transition temperature of about 15 to 18 °C. Solution treatment at 950 °C resulted in the DBTT to be as high as 40 °C, in comparison with the steel treated at 800 °C while all these specimens fractured in a brittle manner, due to a large grain size that originated from annealing at 950 °C. The upper shelf energy seemed to be independent of the Laves phase precipitation. Figure 6.21 shows the microstructural evolution during the

reheating treatment; and from this optical micrograph the grain boundary Laves phase precipitates could be observed. At both 600 and 900 °C, there are few precipitates present as compared to the specimens annealed at 700 and 800 °C. The hardness results in Figure 6.22, show the effect of this Laves phase re-precipitation on the hardness values of the Steel A. The result shows a slight increase in the hardness value at the annealing temperature of 700 °C, then the hardness decreases with annealing at higher temperatures. Comparing these results with those from Figure 6.22, it can be concluded that there is no clear correlation between the Laves phase precipitation and the Charpy upper shelf energy.

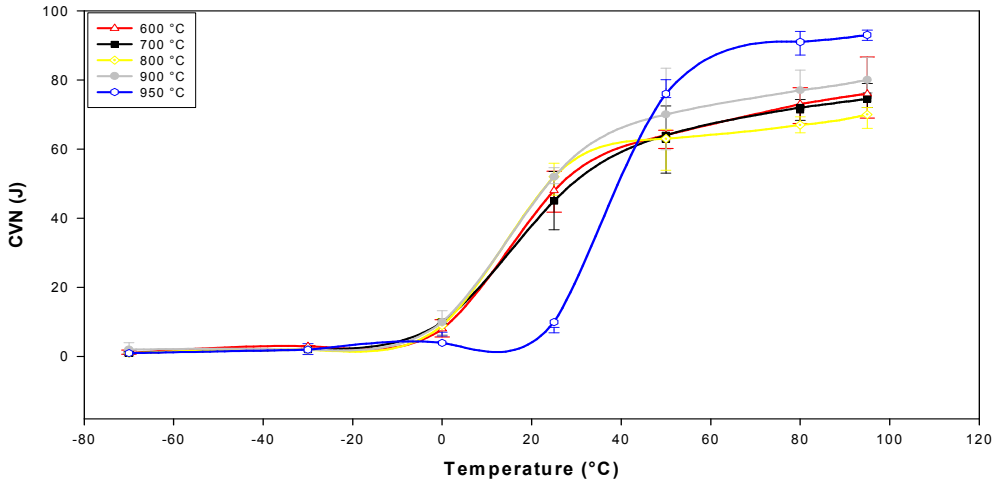

Figure 6.20. Charpy impact energy of Steel A as a function of the test temperature of specimens first solution annealed at 950°C and then re-annealed at different temperatures.

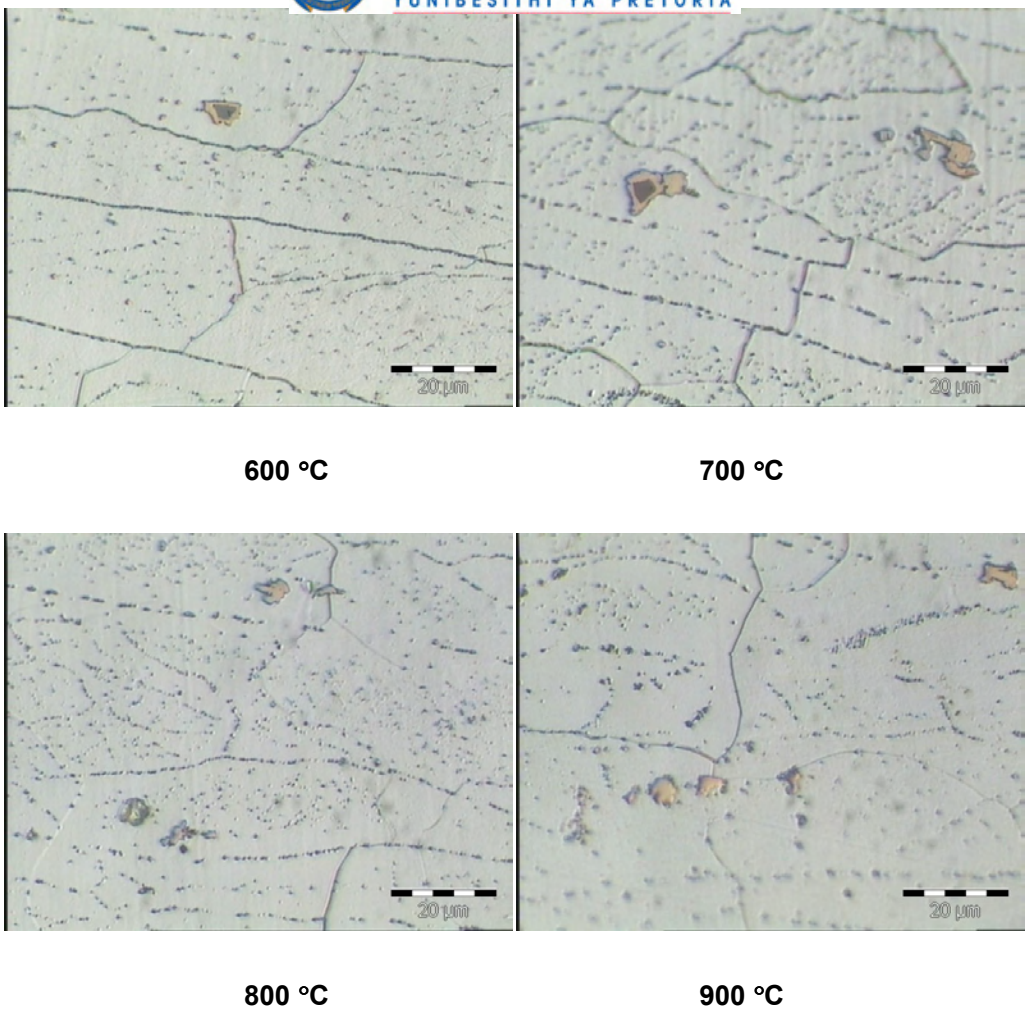

Figure 6.21. Optical microscopy micrographs showing microstructural evolution in Steel A during re – heating treatments after an original solution treatment at 950°C.

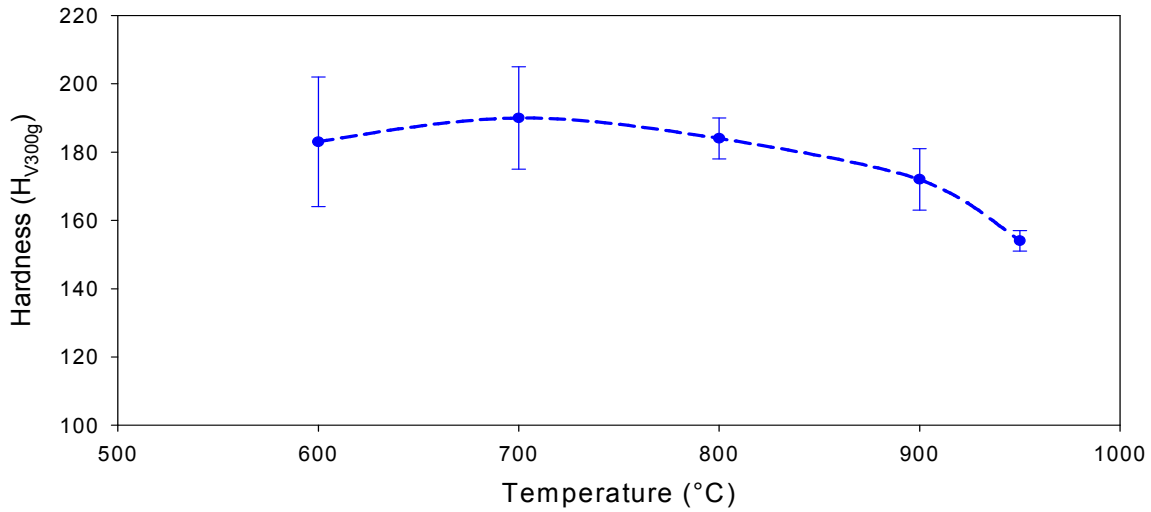

Figure 6.22. Effect of the Laves phase re-precipitation in Steel A on the hardness of the material during embrittlement treatment after an original solution treatment at 950°C.